J. Plasma Phys. (2023), *vol*. 89, 965890601
Published by Cambridge University Press

doi:10.1017/S0022377823001332

Proton and helium ions acceleration in near-critical density gas targets by short-pulse Ti:Sa PW-class laser

J.L. Henares[1,†], P. Puyuelo-Valdes[1], C. Salgado-López[1], J.I. Apiñaniz[1], P. Bradford[2], F. Consoli[3], D. de Luis[1], M. Ehret[1], F. Hannachi[4], R. Hernández-Martín[1], A. Huber[4], L. Lancia[5], M. Mackeviciute[6], A. Maitrallain[4], J.-R. Marquès[5], J.A. Pérez-Hernández[1], C. Santos[1], J.J. Santos[2], V. Stankevic[6], M. Tarisien[4], V. Tomkus[6], L. Volpe[1,7] and G. Gatti[1]

[1]CLPU (Centro de Láseres Pulsados), Edificio M5, Parque Científico USAL, C/Adaja, 8, 37185 Villamayor, Salamanca, Spain

[2]CELIA (Centre Lasers Intenses et Applications), Université de Bordeaux, CNRS, CEA, UMR 5107, 33400 Talence, France

[3]ENEA Fusion and Technologies for Nuclear Safety Department, C.R. Frascati, Via Enrico Fermi 45, Frascati, Rome, Italy

[4]Laboratoire de Physique des Deux Infinis de Bordeaux (LP2I), Université de Bordeaux, CNRS-IN2P3, LP2I, UMR 5797, F-33170 Gradignan, France

[5]LULI, Ecole Polytechnique-CNRS-CEA-Université Paris VI, F-91128 Palaiseau, France

[6]FTMC - Center for Physical Sciences and Technology, Savanoriu av. 231, LT-02300 Vilnius, Lithuania

[7]ETSIAE Universidad Politecnica de Madrid, 28006 Madrid, Spain

(Received 26 September 2023; revised 21 November 2023; accepted 22 November 2023)

The ability to quickly refresh gas-jet targets without cycling the vacuum chamber makes them a promising candidate for laser-accelerated ion experiments at high repetition rate. Here we present results from the first high repetition rate ion acceleration experiment on the VEGA-3 PW-class laser at CLPU. A near-critical density gas-jet target was produced by forcing a 1000 bar H_2 and He gas mix through bespoke supersonic shock nozzles. Proton energies up to 2 MeV were measured in the laser forward direction and 2.2 MeV transversally. He^{2+} ions up to 5.8 MeV were also measured in the transverse direction. To help maintain a consistent gas density profile over many shots, nozzles were designed to produce a high-density shock at distances larger than 1 mm from the nozzle exit. We outline a procedure for optimizing the laser–gas interaction by translating the nozzle along the laser axis and using different nozzle materials. Several tens of laser interactions were performed with the same nozzle which demonstrates the potential usefulness of gas-jet targets as high repetition rate particle source.

Key words: intense particle beams, plasma diagnostics

† Email address for correspondence: jlhenares@clpu.es

1. Introduction

The current development of laser-plasma particle acceleration technology is exhibiting its importance in experiments involving proton and ion particles and the wide applications that they can provide (Daido, Nishiuchi & Pirozhkov 2012; Pommarel *et al.* 2017). Traditional laser-plasma acceleration of protons and ions is performed when a high-power laser (terawatt (TW) and petawatt (PW) power) irradiates a solid target in a well-known acceleration process called target normal sheath acceleration (TNSA) (Borghesi 2014). This acceleration mechanism is capable of generating high-energy particle bunches with energy distributions of several tens of MeV (Macchi, Borghesi & Passoni 2013). Unfortunately, however, solid targets produce a lot of debris and are generally slow to replace, limiting their usefulness in the new generation of femtosecond laser facilities operating at high repetition rates (HRRs). Laser facilities like APOLLON (France) (Burdonov *et al.* 2021), CoReLS (Korea) (Yoon *et al.* 2021), ELI-NP (Romania) (Radier *et al.* 2022), ELI-Beamlines L3-HAPLS (Czech Republic) (Borneis *et al.* 2021), BELLA (USA) (Hakimi *et al.* 2022) or CLPU-VEGA3 (Spain) (Roso 2018) will support shot rates from 1 to 10 Hz. The interest in the possibility of new physics and direct applications due to the increase in the number of generated particles and the capability to deliver high-energy particles in short periods of time triggered the development of alternative targets. Several alternatives to provide HRR targets are currently being developed worldwide to overcome the above-commented limitations: multistage solid targets (Dover *et al.* 2020; Loughran *et al.* 2023), cryogenic ribbons (Margarone *et al.* 2016; Rehwald *et al.* 2023), liquid targets (Hilz *et al.* 2018; Puyuelo-Valdes *et al.* 2022) or gas-jet targets (Sylla *et al.* 2012).

Here we will focus on the development of near-critical density gas-jet targets for laser-plasma ion acceleration. High-density gases can reach near-critical electron densities once fully ionized ($n_c \approx 10^{21}$ cm^{-3} depending on the laser wavelength). The critical density is a region of interest for laser-plasma acceleration for the different acceleration regimes that can be triggered and the enhancement of the coupling efficiency of the laser to the plasma compared to underdense or overdense plasmas. In addition, gas targets have several advantages. The main one is the implicit self-refreshment of the target after the laser interaction which makes them a perfect candidate for high repetition rate operation. They also produce relatively pure ion beams since the gas mix purity can be controlled. Finally, gas targets can be optically probed that makes them interesting to study alternative acceleration schemes and to understand underlying physics.

High-density gas targets have been used for electron acceleration (Faure *et al.* 2004; Geddes *et al.* 2004; Mangles *et al.* 2004) and high repetition rate operation is now available (Guénot *et al.* 2017; Faure *et al.* 2018). Laser-plasma ion acceleration has been moderately studied with CO_2 lasers ($\lambda = 10$ μm, $n_c = 1.12 \times 10^{19}$ cm^{-3}) (Palmer *et al.* 2011; Haberberger *et al.* 2012; Tresca *et al.* 2015). Haberberger *et al.* (2012) have demonstrated the production of proton beams up to 20 MeV with an extremely narrow energy spread. Collisionless shockwave acceleration (CSA) was identified as the main acceleration mechanism in that experiment (Fiuza *et al.* 2012). Then, the interaction with Nd:YAG lasers ($\lambda = 1$ μm, $n_c = 1 \times 10^{21}$ cm^{-3}) was studied by several groups leading to acceleration of protons up to 600 keV (Chen *et al.* 2017), and Puyuelo-Valdes *et al.* (2019*a*) measured protons up to 6 MeV with a slightly peaked spectra and He^{2+} ions up to 15 MeV in the transverse direction (Puyuelo-Valdes *et al.* 2019b). Hole boring (HB) (Wilks *et al.* 1992) was identified as the main acceleration mechanism. Despite excellent results, experiments carried out with CO_2 and Nd:YAG are limited to low repetition rates (less than a few shots per hour). With the recent development of HRR Ti:Sa laser systems ($\lambda = 800$ nm, $n_c = 1.75 \times 10^{21}$ cm^{-3}), a significant research effort is

https://doi.org/10.1017/S0022377823001332 Published online by Cambridge University Press

now devoted to producing ion beams with high energy and high average flux, such as might be useful for medical isotope production (Spencer *et al.* 2001) or cancer therapy (Ledingham *et al.* 2014). Sylla *et al.* (2013) reported transverse acceleration of He^{+} ions up to 250 keV with a Ti:Sa laser. They optically probed the laser plasma interaction zone, which revealed channelling of the laser, self-focusing and an efficient energy deposition at the point of laser beam collapse. Singh *et al.* (2020) measured protons and He^{2+} ions up to 750 keV in the transverse direction, characterized by an exponentially decaying spectra and accelerated through mass-dependent radial CSA. Recently, an experimental campaign was carried out at CLPU-VEGA3 by Ospina-Bohórquez *et al.* (2023) where alpha particles were detected with $\approx$1 MeV amu^{-1} at 17°. The experiment was supported by simulations that show acceleration from a CSA-type mechanism at the rapidly expanding walls of the laser-induced plasma channel. Some interesting ideas are being developed such as tailoring the gas density profile to optimize the acceleration process (Marquès *et al.* 2021) or asymmetric nozzles (Rovige *et al.* 2021). Here we present the successful acceleration of multi-MeV protons and He^{2+} ions at a high repetition rate Ti:Sa PW-class laser facility. This was achieved via optimization of the laser interaction through interferometry and transverse 2w-emission imaging. A study of nozzle damage is also presented, which is the main limitation for producing high repetition rate laser-driven ion beams for various applications.

2. Experimental set-up

The experiment was carried out in the VEGA3 laser facility at CLPU (Spain). The laser system consists of a Ti:Sa laser ($\lambda = 800$ nm) that can deliver energies up to 30 J, temporal duration up to 30 fs and up to 1 Hz repetition rate. The laser beam is focused by an $f/11$ off-axis parabolic mirror to a spot of 12 μm full-width at half-maximum (FWHM). The energy on target is extrapolated from calibrations recorded at low energy, and the focal spot at high energy is estimated to remain the same. We estimate that 21 % of the energy on target is within the first Airy disk at FWHM, based on images of the focal spot taken at low energy and taking into account compressor and transport loses. This gives an effective energy of approximately 6.3 J on target. The laser energy and pulse duration are measured on-shot (the latter using a second harmonic autocorrelator system). The laser energy remained constant throughout this study but the temporal pulse duration was fixed up to a maximum of 300 fs for the whole experiment (negative chirp). The reason for using 300 fs was to compare with the results obtained in picosecond laser pulse facilities (such as the experiment by Puyuelo-Valdes *et al.* (2019*a*)) and then to move to shorter pulse durations. However, the laser beam time duration for this experimental campaign was not enough to perform the full study. The intensity used in this study was 1.85×10^{19} W cm^{-2}. The laser contrast of VEGA3 is up to 10^{-12} at 0.1 ns with no significant pre-pulses that could ionize and thus modify the accelerating properties of the gas target.

The set-up of the experiment is shown in figure 1. The gas used is a mixture of He (97 %) and H_2 (3 %). The gas target consist of a supersonic gas-jet nozzle that produces a high-density region away from the nozzle exit. The gas travels vertically out of the nozzle along the z-axis, where zero distance is defined at the nozzle surface (Henares *et al.* 2018). This target can produce near-critical electron densities when fully ionized. For reference, the critical density is $n_c = 1.74 \times 10^{21}$ cm^{-3} for our Ti:Sa laser. The nozzle design consists of a convergent-divergent geometry with a straight duct at the exit (Rovige *et al.* 2021). The hydrodynamic flow follows a supersonic expansion due to the convergent-divergent region whereas the straight part makes the gas converge, producing a sharp maximum transverse density profile from the accumulation of oblique shocks. The gas-jet nozzle is mounted on a Clark Cooper solenoid valve EX30 that can provide continuous or pulsed gas flux. The

https://doi.org/10.1017/S0022377823001332 Published online by Cambridge University Press

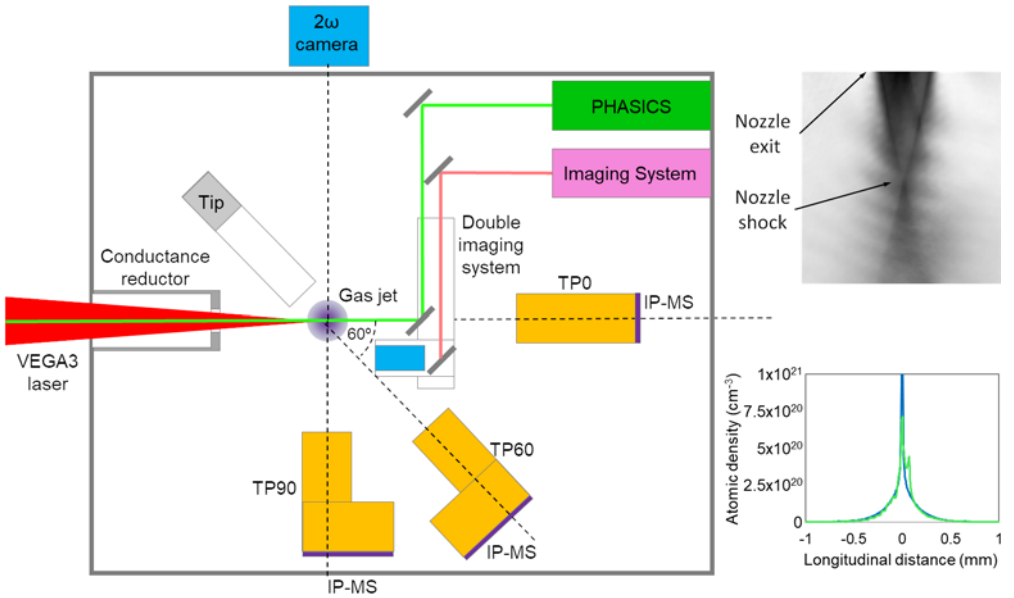

FIGURE 1. Set-up of the experiment and diagnostics in the VEGA3 experimental chamber (see text for details). The graphics on the right show (top) a phase map image of the shock obtained with PHASICS and (bottom) the density profiles obtained by computational fluid dynamics simulations of a shock nozzle at $Z = 900$ μm (blue) and interferometric density measurement (green).

high density is reached by using 1000 bars inlet pressure delivered by a Haskel gas booster model AGT-62/152. The nozzle is designed to produce a high-density shock at distances ranging in Z values from 900 to 1500 mm depending on the construction parameters. The generated density profile was calculated using computational fluid dynamics (CFD) simulations by the FLUENT software (ANSYS FLUENT Academic Research Mechanical 2022), which numerically solves the Navier–Stokes equations on a discrete grid (additional information can be found in Henares *et al.* 2019). Peak atomic densities in the interval between 1×10^{21} cm^{-3} and 0.5×10^{21} cm^{-3} were obtained for lower Z distances and higher Z distances of the shock, respectively. Tungsten and UVFS fused silica materials were studied for the nozzle construction. The gas target is mounted in a *XYZ* axis motor platform to finely position the shock at the interaction point with respect to the calculated one.

Three Thomson parabola (TP) spectrometers, placed at 0°, 60° and 90° with respect to the laser forward axis, were used to characterize ion emission from the target. A TP consists of a magnetic dipole followed by a pair of electric plates which allow to measure the energy distributions of different ion species. BAS-MS and BAS-SR imaging plates (IPs) were used to record the particles and they were analysed using a FUJIFILM FLA-7000 reader. The IPs were protected by aluminized Mylar foils of 2 μm thickness. The IP response functions to ions are taken from Bonnet *et al.* (2013). The sensitivity limitations (including Mylar protective foils) for IP-MS are 0.78 MeV for protons and 2.7 MeV for He ions, and for IP-SR are 0.62 MeV for protons and 2.5 MeV for He ions. TPs were calibrated by measuring the magnetic field between the plates and then comparing the expected particle trajectories with results from particle accelerators. TPs were positioned at 35 cm from the gas target with 500 μm-diameter entrance pinholes.

https://doi.org/10.1017/S0022377823001332 Published online by Cambridge University Press

A high voltage was used to deflect the particles. They will be referenced as TP0 (0°), TP60 (60°) and TP90 (90°). More specific information of TP0 can be found from Salgado-López *et al.* (2022), and for TP60 and TP90 from Baccou (2016).

The imaging system consists of a microscope to calculate the focal spot and to determine the pointing. In the same path, a wavefront sensor PHASICS SID4 interferometer (Plateau *et al.* 2010) was installed to estimate the rate of damage of the nozzle after the shot, to correlate the reference of the laser interaction point with the position of the shock nozzle and, in some cases, to measure the real density before each shot. Using the latter allowed to finely position the shock in transverse and vertical planes with respect to the laser axis within an error of 3 μm. The longitudinal position of the shock nozzle was arranged by a camera at 90° with respect to the laser axis. This camera was also used to set a diagnostic to measure the 2ω emission of the plasma generated by the laser interaction.

3. Results

Optimization of the laser interaction was carried out in two stages. Before the laser shot, the wavefront sensor PHASICS SID4 measured the density profile and the position of the shock was determined. After the laser shot, the 2ω diagnostic was used to fine optimize the intensity of the emission of the plasma generated by the interaction. Figure 2 shows an example of the optimization in *XYZ* directions (longitudinal *L*, transversal *T* and vertical *V*, respectively). One should note that vertical movements *V* are relative movements with respect to the reference and they are different to the absolute distance of the shock from the nozzle exit (*Z*). The nozzle assembly was moved in all directions and major changes in the emission were observed when exiting the high-density region. The transverse sensitivity of the interaction using shock nozzles was observed to be very high: no signal was observed outside of a 100 μm range. The range in longitudinal position to obtain a clear interaction was larger (estimated to be approximately 200 μm) probably due to the laser interaction in the density profile wings and the laser Rayleigh length (>200 μm). It was not possible to determine if the highest efficiency was found when the laser was focused at the centre of the density profile of the gas jet or in the rising slope (the latter effect was observed using De Laval nozzles in previous experiments). The vertical optimization range was estimated to be larger, but no reliable measurement could be performed and nozzles rapidly degraded when approaching the interaction point to the nozzle exit.

For every shot and at each angle, the traces of protons, He^{1+} and He^{2+}, were analysed. For each ion species, a parabolic trace and a background zone close to it were isolated on the IP. The background was carefully subtracted for each parabola. He^{1+} traces were not observed, so it is possible to consider that the high-intensity laser fully ionized both gases during the interaction. Since the IPs are passive detectors, the accumulation of several laser interactions was performed. To avoid fading effects, the IPs were scanned within 20 minutes after the laser interaction.

3.1. H^+ *acceleration*

Figures 3(*a*)–3(*c*) show representative proton energy spectra for angles 0°, 60° and 90° in an accumulation of five shots using IP-MS. All shots performed in the campaign showed proton signal in the 90° and 60° detectors, but only some shots could accelerate protons in the forward direction. Figure 3(*a*) presents the energy spectra detected at 0°. It is characterized by a decreasing exponential up to 2 MeV and up to 10^{10} protons/MeV/sr directed along the laser propagation axis. The energy spectra at 60° and 90° show a sharp cut-off at 1.75 and 2.2 MeV, respectively (figures 3*b* and 3*c*). It is important to note the two exponential distributions in the energy spectrum at 90° (discussed later), the first one

https://doi.org/10.1017/S0022377823001332 Published online by Cambridge University Press

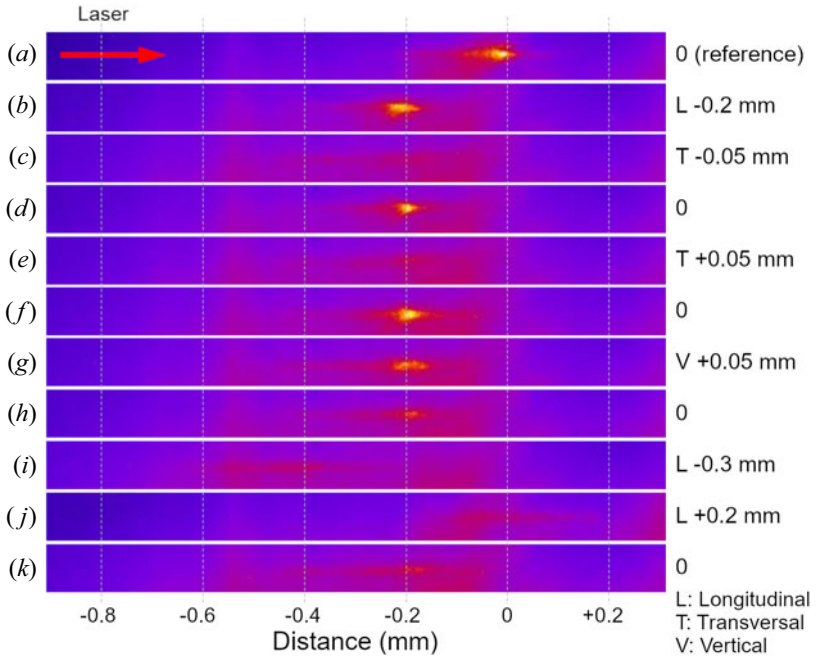

FIGURE 2. Camera recording the 2ω plasma interaction region at 90° with respect to the laser axis (the red arrow indicates the laser direction). The pseudo-colour images are only processed assigning a lookup table. The first position in panel (*a*) is where the maximum density is expected by interferometry ($Z = 1350$ μm). The laser is fixed at 0 position and the nozzle has been moved to different positions to optimize the signal (relative movements with respect to the reference): (*a*) starting point; (*b*) nozzle moved longitudinal (laser axis) −0.2 mm; (*c–f*) nozzle moved transversely −0.05 mm, centred and +0.05 mm, and back again to the centred position, respectively; (*g*) nozzle moved up to 1400 mm (+0.05 mm); (*h*) centred again in vertical, some damage starts to be seen; (*i*, *j*) nozzle moved longitudinal (laser axis) −0.3 mm and then +0.2 mm; (*k*) nozzle centred again in the maximum signal position. The nozzle now shows evidence of damage.

decreasing (if extrapolated) at 1.75 MeV and the second at 2.2 MeV, and the increase of the number of particles up to 10^{12} protons/MeV/sr for the lower energies, compared to the value of 10^{10} protons/MeV/sr detected at 60° at the same energies. Figure 3(*d*) is a special case where an isolated bunch was observed at 60° angle showing energies up to 2.3 MeV, with a maximum number of particles of 10^{10} protons/MeV/sr at approximately 1.75 MeV. The energy spectra at 90° of this case showed a decreasing exponential up to 1.5 MeV (not shown).

3.2. *He^{2+} acceleration*

Only perfectly 2ω-optimized laser-target interactions showed He signal in the 90° detector, while no He signal was observed at 60° and 0°. Figure 4(*a*) shows the results of the energy spectrum of He ions at 90°. Figure 4(*b*) shows the scanned IP-SR with the expected parabolas path to distinguish species. The He^{2+} and H^{+} traces do not overlap. He^{1+} was not observed and full ionization was considered without recombinations. The maximum He^{2+} energies were 5.8 MeV with a number of particles up to 10^{9} particle/MeV/sr.

https://doi.org/10.1017/S0022377823001332 Published online by Cambridge University Press

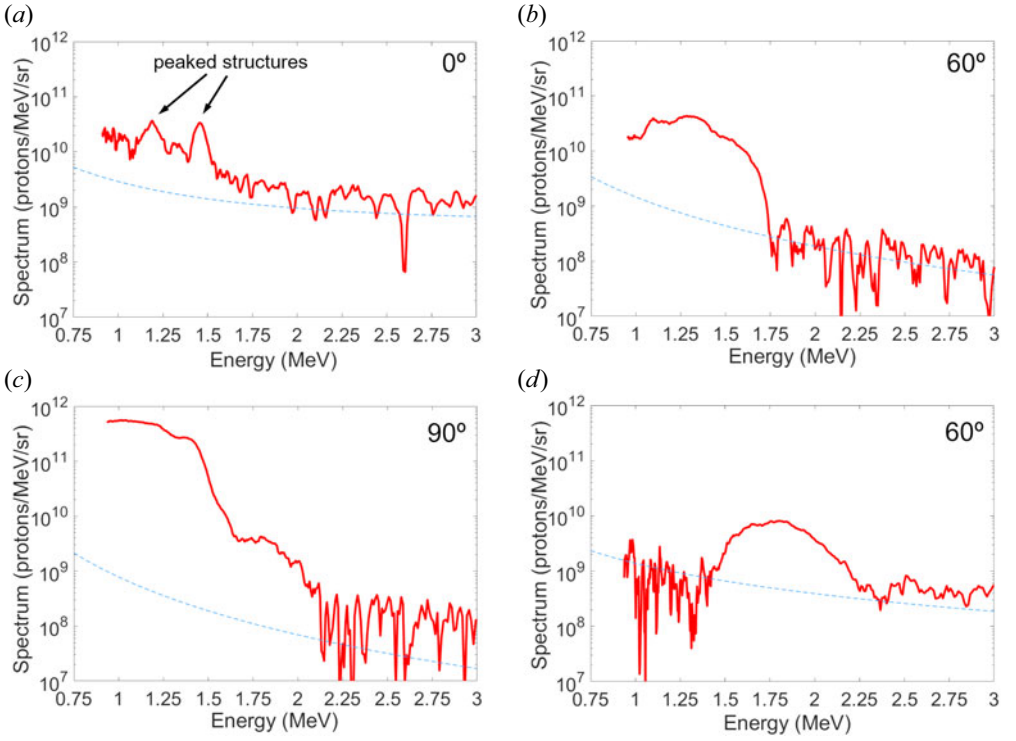

FIGURE 3. Proton energy spectra accumulated over five shots and measured at different detection angles with IP-MS: (*a*) 0° with maximum energies of 2 MeV; (*b*) 60° with maximum energies of 1.75 MeV and (*c*) 90° with maximum energies of 2.2 MeV. (*d*) Spectrum accumulated over 10 shots measured at 60° showing an energy bunch up to 2.3 MeV. The blue-dashed line marks the background noise spectrum.

3.3. *Electron acceleration*

In addition, the electron signature was observed along the forward direction using a larger IP-MS in the TP spectrometer (see figure 5). Since the TP is not built to specifically measure electrons, the background noise was too high for spectrum reconstruction. The maximum electron energies were calculated according to the minimum visible signal over the background. This estimation gave maximum energies of approximately 70 MeV and the minimum energies observed were 32 MeV, where the trace exits the IP. This maximum energy value is well above the expected ponderomotive scaling defined by Wilks *et al.* (2001), but this enhancement is the clear imprint of a near-critical interaction seen by Debayle *et al.* (2017). Specific set-up of the TP will be needed to measure the electron spectrum in the propagation axis.

4. Discussion

Transverse acceleration of protons and ions can be explained by laser self-focusing, collapse and electron expulsion in radial directions (Krushelnick *et al.* 1999). Then the ponderomotive force distributes the electron perpendicular to the laser beam direction, and the ions are pulled and subsequently accelerated. This behaviour has been seen in several references (Sarkisov *et al.* 1999; Sylla *et al.* 2013; Puyuelo-Valdes *et al.* 2019b; Ospina-Bohórquez 2022) in He gas-jet targets and gives a decreasing exponential energy

https://doi.org/10.1017/S0022377823001332 Published online by Cambridge University Press

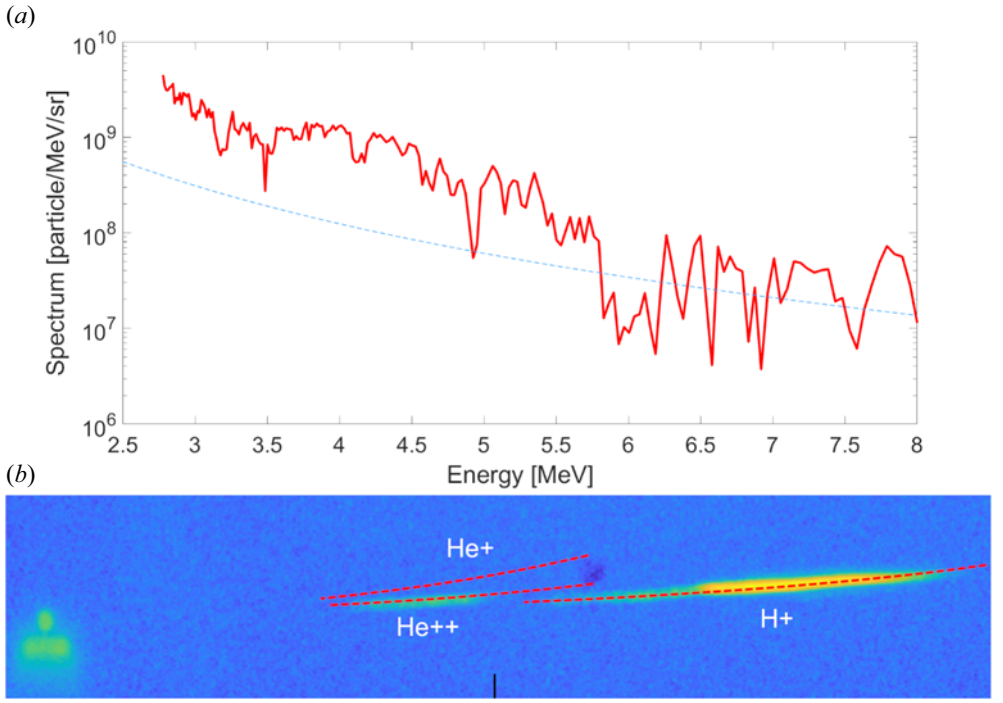

FIGURE 4. (*a*) He^{2+} energy spectrum measured at 90° with IP-SR showing a maximum energy up to 5.8 MeV (accumulation of three shots). The blue-dashed line indicates the background noise spectrum. (*b*) Scanned IP-SR that shows the different parabolic traces of proton and He^{2+}. Expected deflection is indicated by a red dashed line (He^{1+} is also indicated to distinguish species). The He right part of the trace stops in the cut-off for the sensitivity of IP-SR (indicated by a black line). The zero deflection is shown in the circle coming from direct X-rays. The exit of the nozzle is also visible due to X-ray imaging by the pinhole.

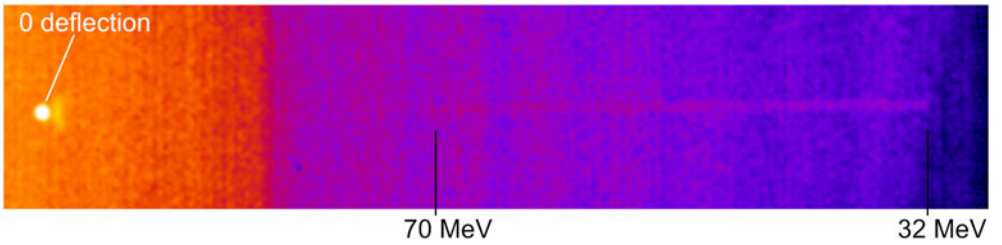

FIGURE 5. Electron trace in a scanned IP-MS at 0°. The voltage of the TP was set to 0. The pseudo-colour image is processed assigning a lookup table and selecting the appropriate range of brightness/contrast for clarification.

spectrum as we have measured. At 0°, this signal is superimposed by some peaks (indicated by arrows in figure 3*a*) that could be the mark of an alternative acceleration process such as CSA or HB. Peaked structures have also been observed by Wei *et al.* (2004) where the detector spectrometer was placed at 100°. They considered this signal characteristic of laser-driven CSA. The two-component spectrum at 90° in figure 3(*c*) could also be the mark of alternative acceleration schemes that compete with each

https://doi.org/10.1017/S0022377823001332 Published online by Cambridge University Press

other. This energy spectrum could be related to the bunched spectra measured at 60° in figure 3(*d*) if the low-energy part is removed. If this is the case, the formation of a collisionless shockwave could accelerate the protons to twice the shock velocity (Silva *et al.* 2004).

Note that background noise in the 0° detector was caused by electric arcs between the high-voltage plates of the TP. These discharges come from electric breakdown due to the increase of pressure in the experimental chamber during the interaction. Other angles showed less background noise due to a better isolation of the TPs. The choice of BAS-MS and BAS-SR IPs was found to be a problem for measuring He ions since their sensitivity for low energies is approximately 3 MeV (due to their protection layers). For future experiments, BAS-TR IP will be used as they have a minimum sensitivity of approximately 0.8 MeV for He ions (since the protection layer is not present). A second option will be to isolate the TP equipped by a micro channel plate (MCP) detector in an independent chamber with differential vacuum. The MCP detector has the advantage of increased sensitivity and possibility of HRR operation.

5. High repetition rate operation

Nozzle survival is a vitally important issue for HRR experiments. The strong interaction of the high-power laser with matter provokes a plasma that expands and interacts with the nozzle duct. This irreversibly damages the nozzle by the modification of its internal geometry. It is important to note that stainless steel, copper or polymers only stand one shot under these extreme conditions. Tungsten and UV fused silica nozzles were explored as nozzle materials to resist the plasma expansion damage. Figure 6 shows the density profiles of two tungsten nozzles after several laser interactions compared with the theoretical density profile given by the simulations in undamaged conditions. It is possible to see that after 25 shots, the density profile at the interaction distance is still reasonable and close to the predicted one, so tungsten is a suitable material to use in these types of experiment. Figure 7 shows scanning electron microscopy (SEM) pictures of the external exit diameter of the nozzles comparing an undamaged nozzle (figure 7*a*) with nozzles used during this campaign. The nozzle shown in figure 7(*b*) has been used for 21 laser shots and still could be used even if the density profile is slightly deteriorated. The nozzle shown in figure 7(*c*) has been used in 41 laser shots and was clearly damaged. In the latter, the straight duct is completely deformed, and the gas shock is faint and its position ambiguous.

However, UVFS fused silica has been also tested as nozzle material. The fused silica nozzle resisted the 1000 bar backing pressure, but unfortunately the nozzle was shot at 400 μm due to an error and the nozzle was destroyed (figure 7*d* shows a slice of material removed after the laser shot). It was concluded that the nozzle could not resist the plasma shockwave and subsequent heating. Anyway, this material is expected to resist if used at higher Z distances and it will be tested in future campaigns. We consider that the extrapolation is not possible comparing the resistance of the fused silica nozzle with the tungsten nozzle at 1 mm above the outlet, where tungsten nozzles have been operated.

A second problem found for high repetition rate operation is the vacuum degradation of the experimental chamber. This can cause problems in the diagnostics using high voltages (sparks) and the absorption of particles if running continuously. This caused problems in our main detectors (IPs) since it blurred the main signal increasing the background noise as previously mentioned. Mylar protection was not enough to stop the light from the sparks due to its transparent nature. In addition, the extraction of the residual gas limited the maximum repetition rate of the experiment to have a proper vacuum environment (below 10^{-5} mbar) using a 1000 bar gas target. In these conditions, it was possible to perform consecutive laser shots with a repetition rate of 2 min^{-1}, which represents a

https://doi.org/10.1017/S0022377823001332 Published online by Cambridge University Press

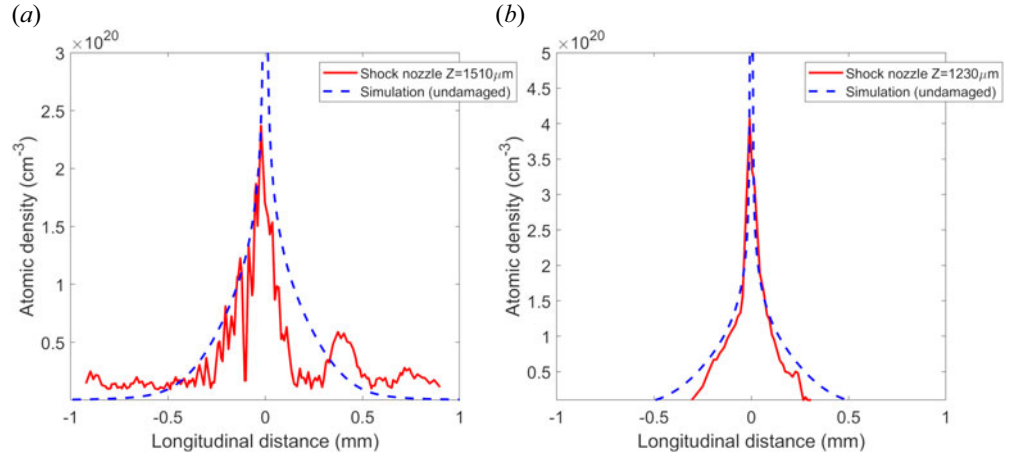

FIGURE 6. Density profile comparison between measurements performed by interferometry and simulations at two distances from the nozzle exit using two shock nozzles: (*a*) $Z = 1510$ μm, after 19 shots and (*b*) $Z = 1230$ μm, after 25 shots. The central high-density region is complicated to reconstruct due to the error using the Abel inversion at the symmetry axis. Anyway, we can clearly see that the high-density shock still resists in spite of the damage and the agreement with a theoretical undamaged nozzle is good.

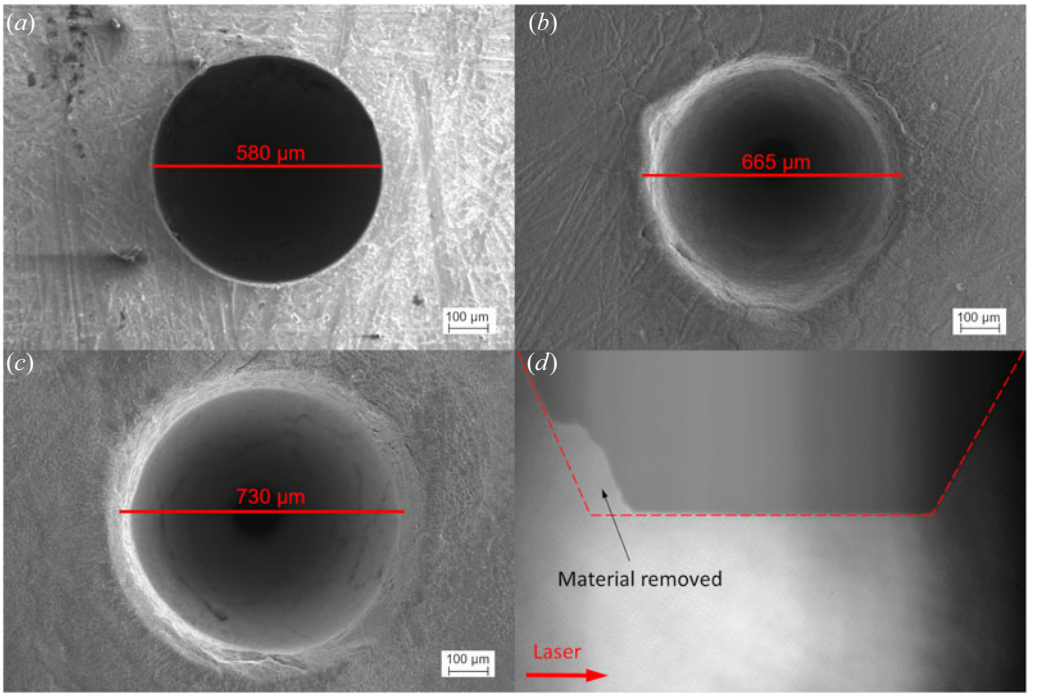

FIGURE 7. Scanning electron microscopy (SEM) pictures of the exit of the nozzles: (*a*) tungsten nozzle not used; (*b*) tungsten nozzle used in 21 laser shots; (*c*) tungsten nozzle used in 41 laser shots. The straight duct is clearly damaged. (*d*) Side picture of a UVFS fused silica nozzle after one shot at $Z = 400$ μm. The original profile is marked by a red dashed line.

https://doi.org/10.1017/S0022377823001332 Published online by Cambridge University Press

significant advance compared with present state-of-art of laser-plasma acceleration of protons in gases. There is room for improvement if the residual gas is quickly extracted (via a gas catcher or isolation of the interaction region). This result opens the possibility of automatization and control of the particle source at HRR (Feister *et al.* 2023).

6. Conclusion

In conclusion, maximum proton energies of 2.2 MeV and 1.75 MeV were obtained at 90° and 60°, respectively, and optimization has been successfully reached to obtain forward proton acceleration with maximum energies of 2 MeV. In addition, bunched proton distributions at 60° were also observed. In the case of He^{2+}, maximum energies were obtained of approximately 5.8 MeV only in the transverse direction. Finally, electrons were measured up to 70 MeV in the forward direction. It was proven that the optimization of the interaction position (via both interferometry and 2ω emission) was fundamental to enhance particle acceleration at HRR. In addition, it a technical milestone was established with 41 shots performed with one single nozzle until fully damaged with a maximum repetition rate of 2 min^{-1}. It was shown that high-resistance materials and higher distances from the outlet could enhance the nozzle survival. A study involving several 100s of shots in optimized conditions should be needed to definitely demonstrate the HRR potentials of the system. In future experiments, we plan to decrease the laser pulse duration down to 30 fs, and to scan densities slightly above and below the critical density to identify the best parameters for optimization of the ion spectral profile. Particle-in-cell (PIC) simulations will be essential to validate and help to understand these results, though these simulations have a high computational cost due to the large interaction regions that are needed to completely include the gas expansion. We have identified a need of diagnostic development and improvement of the gas extraction method to increase the repetition rate of the source, but the potential usefulness of gas-jet targets for an HRR particle source have been demonstrated.

Acknowledgements

We would like to express our gratitude to the laser and engineering teams at CLPU without whose support this work would not have been possible.

Editor Victor Malka thanks the referees for their advice in evaluating this article.

Declaration of interest

The authors report no conflict of interest.

Funding

This work received funding from Grant PID2021-125389OA-I00 funded by MCIN/AEI/10.13039/501100011033/FEDER, UE and by "ERDF A way of making Europe", by the "European Union".

REFERENCES

ANSYS FLUENT ACADEMIC RESEARCH MECHANICAL 2022 Release 22.1.

BACCOU, C. 2016 Initiation de réactions nucléaires par des protons accélérés par laser. PhD thesis, Universite Paris Saclay.

BONNET, T., COMET, M., DENIS-PETIT, D., GOBET, F., HANNACHI, F., TARISIEN, M., VERSTEEGEN, M. & ALEONARD, M.M. 2013 Response functions of fuji imaging plates to monoenergetic protons in the energy range 0.6–3.2 MeV. *Rev. Sci. Instrum.* **84** (1), 013508.

https://doi.org/10.1017/S0022377823001332 Published online by Cambridge University Press

Borghesi, M. 2014 Laser-driven ion acceleration: state of the art and emerging mechanisms. *Nucl. Instrum. Meth. Phys. Res. Sec.* A*: Accel. Spectrom. Detect. Assoc. Equip*. **740**, 6–9, and references therein.

Borneis, S., Laštovička, T., Sokol, M., Jeong, T.-M., Condamine, F., Renner, O., Tikhonchuk, V., Bohlin, H., Fajstavr, A., Hernandez, J.-C., *et al.* 2021 Design, installation and commissioning of the eli-beamlines high-power, high-repetition rate hapls laser beam transport system to p3. *High Power Laser Sci. Engng* **9**, e30.

Burdonov, K., *et al.* 2021 Characterization and performance of the apollon short-focal-area facility following its commissioning at 1 pw level. *Matt. Radiat. Extremes* **6**.

Chen, S.N., Vranic, M., Gangolf, T., Boella, E., Antici, P., Bailly-Grandvaux, M., Loiseau, P., Pépin, H., Revet, G., Santos, J.J., Schroer, A.M., Starodubtsev, M., Willi, O., Silva, L.O., d'Humières, E. & Fuchs, J. 2017 Collimated protons accelerated from an overdense gas jet irradiated by a 1 μm wavelength high-intensity short-pulse laser. *Sci. Rep*. **7** (13505), 2045–2322.

Daido, H., Nishiuchi, M. & Pirozhkov, A.S. 2012 Review of laser-driven ion sources and their applications. *Rep. Prog. Phys*. **75** (5), 056401.

Debayle, A., Mollica, F., Vauzour, B., Wan, Y., Flacco, A., Malka, V., Davoine, X. & Gremillet, L. 2017 Electron heating by intense short-pulse lasers propagating through near-critical plasmas. *New J. Phys*. **19** (12), 123013.

Dover, N.P., *et al.* 2020 Demonstration of repetitive energetic proton generation by ultra-intense laser interaction with a tape target. *High Energy Density Phys*. **37**, 100847.

Faure, J., Glinec, Y., Pukhov, A., Kiselev, S., Gordienko, S., Lefebvre, E., Rousseau, J.P., Burgy, F. & Malka, V. 2004 A laser-plasma accelerator producing monoenergetic electron beams. *Nature* **431** (7008), 541–544, we acknowledge support from the European Community Research Infrastructure Activity under the FP6 'Structuring the European Research Area' programme (CARE) and from the German Scientific Council (DFG).

Faure, J., Gustas, D., Guénot, D., Vernier, A., Böhle, F., Ouillé, M., Haessler, S., Lopez-Martens, R. & Lifschitz, A. 2018 A review of recent progress on laser-plasma acceleration at kHz repetition rate. *Plasma Phys. Control. Fusion* **61** (1), 014012.

Feister, S., Cassou, K., Dann, S., Döpp, A., Gauron, P., Gonsalves, A.J., Joglekar, A., Marshall, V., Neveu, O., Schlenvoigt, H.-P., *et al.* 2023 Control systems and data management for high-power laser facilities. *High Power Laser Sci. Engng* **11**, e56.

Fiuza, F., Stockem, A., Boella, E., Fonseca, R.A., Silva, L.O., Haberberger, D., Tochitsky, S., Gong, C., Mori, W.B. & Joshi, C. 2012 Laser-driven shock acceleration of monoenergetic ion beams. *Phys. Rev. Lett*. **109**, 215001.

Geddes, C.G.R., Toth, C., van Tilborg, J., Esarey, E., Schroeder, C.B., Bruhwiler, D., Nieter, C., Cary, J. & Leemans, W. 2004 High-quality electron beams from a laser wakefield accelerator using plasma-channel guiding. *Nature* **431**.

Guénot, D., Gustas, D., Vernier, A., Beaurepaire, B., Böhle, F., Bocoum, M., Lozano, M., Jullien, A., Lopez-Martens, R., Lifschitz, A. & Faure, J. 2017 Relativistic electron beams driven by khz single-cycle light pulses. *Nat. Photonics* **11**, 293.

Haberberger, D., Tochitsky, S., Fiuza, F., Gong, C., Fonseca, R.A., Silva, L.O., Mori, W.B. & Joshi, C. 2012 Collisionless shocks in laser-produced plasma generate monoenergetic high-energy proton beams. *Nature Phys*. **8**.

Hakimi, S., Obst-Huebl, L., Huebl, A., Nakamura, K., Bulanov, S.S., Steinke, S., Leemans, W.P., Kober, Z., Ostermayr, T.M., Schenkel, T., Gonsalves, A.J., Vay, J.-L., van Tilborg, J., Toth, C., Schroeder, C.B., Esarey, E. & Geddes, C.G.R. 2022 Laser–solid interaction studies enabled by the new capabilities of the iP2 BELLA PW beamline. *Phys. Plasmas* **29** (8), 083102.

Henares, J.L., Puyuelo-Valdes, P., Hannachi, F., Ceccotti, T., Ehret, M., Gobet, F., Lancia, L., Marquès, J.-R., Santos, J.J., Versteegen, M. & Tarisien, M. 2019 Development of gas jet targets for laser-plasma experiments at near-critical density. *Rev. Sci. Instrum*. **90** (6), 063302.

https://doi.org/10.1017/S0022377823001332 Published online by Cambridge University Press

HENARES, J.L., TARISIEN, T., PUYUELO, P., MARQUÈS, J.-R., NGUYEN-BUI, T., GOBET, F., RAYMOND, X., VERSTEEGEN, M. & HANNACHI, F. 2018 Optimization of critical-density gas jet targets for laser ion acceleration in the collisionless shockwave acceleration regime. *J. Phys.: Conf. Ser*. **1079** (1), 012004.

HILZ, P., OSTERMAYR, T.M., HUEBL, A., BAGNOUD, V., BORM, B., BUSSMANN, M., GALLEI, M., GEBHARD, J., HAFFA, D., HARTMANN, J., KLUGE, T., LINDNER, F.H., NEUMAYR, P., SCHAEFER, C.G., SCHRAMM, U., THIROLF, P.G., RÖSCH, T.F., WAGNER, F., ZIELBAUER, B. & SCHREIBER, J. 2018 Isolated proton bunch acceleration by a petawatt laser pulse. *Nat. Commun*. **9** (1).

KRUSHELNICK, K., CLARK, E.L., NAJMUDIN, Z., SALVATI, M., SANTALA, M.I.K., TATARAKIS, M., DANGOR, A.E., MALKA, V., NEELY, D., ALLOTT, R. & DANSON, C. 1999 Multi-mev ion production from high-intensity laser interactions with underdense plasmas. *Phys. Rev. Lett*. **83**, 737–740.

LEDINGHAM, K.W.D., BOLTON, P.R., SHIKAZONO, N. & MA, C.-M.C. 2014 Towards laser driven hadron cancer radiotherapy: a review of progress. *Appl. Sci*. **4** (3), 402–443.

LOUGHRAN, B., STREETER, M.J.V., AHMED, H., ASTBURY, S., BALCAZAR, M., BORGHESI, M., BOURGEOIS, N., CURRY, C.B., DANN, S.J.D., DIIORIO, S., *et al.* 2023 Automated control and optimization of laser-driven ion acceleration. *High Power Laser Sci. Engng* **11**, e35.

MACCHI, A., BORGHESI, M. & PASSONI, M. 2013 Ion acceleration by superintense laser-plasma interaction. *Rev. Mod. Phys*. **85**, 751–793, and references therein.

MANGLES, S.P.D., MURPHY, C.D., NAJMUDIN, Z., THOMAS, A.G.R., COLLIER, J.L., DANGOR, A.E., DIVALL, E.J., FOSTER, P.S., GALLACHER, J.G., HOOKER, C.J., JAROSZYNSKI, D.A., LANGLEY, A.J., MORI, W.B., NORREYS, P.A., TSUNG, F.S., VISKUP, R., WALTON, B.R. & KRUSHELNICK, K. 2004 Monoenergetic beams of relativistic electrons from intense laser-plasma interactions. *Nature* **431** (7008), 535–538.

MARGARONE, D., *et al.* 2016 Proton acceleration driven by a nanosecond laser from a cryogenic thin solid-hydrogen ribbon. *Phys. Rev.* X **6**, 041030.

MARQUÈS, J.-R., *et al.* 2021 Over-critical sharp-gradient plasma slab produced by the collision of laser-induced blast-waves in a gas jet: application to high-energy proton acceleration. *Phys. Plasmas* **28** (2), 023103.

OSPINA-BOHÓRQUEZ, V. 2022 Ion acceleration from high-intensity laser interactions with quasi-critical-gas targets: experiments and numerical simulations. PhD thesis, Universite de Bordeaux and Universidad de Salamanca.

OSPINA-BOHÓRQUEZ, V., *et al.* 2023 Laser-driven ion and electron acceleration from near-critical density gas targets: towards high-repetition rate operation in the 1 pw, sub-100 fs laser interaction regime. *Phys. Rev. Res*. (submitted).

PALMER, C.A.J., DOVER, N.P., POGORELSKY, I., BABZIEN, M., DUDNIKOVA, G.I., ISPIRIYAN, M., POLYANSKIY, M.N., SCHREIBER, J., SHKOLNIKOV, P., YAKIMENKO, V. & NAJMUDIN, Z. 2011 Monoenergetic proton beams accelerated by a radiation pressure driven shock. *Phys. Rev. Lett*. **106**, 014801.

PLATEAU, G.R., MATLIS, N.H., GEDDES, C.G.R., GONSALVES, A.J., SHIRAISHI, S., LIN, C., VAN MOURIK, R.A. & LEEMANS, W.P. 2010 Wavefront-sensor-based electron density measurements for laser-plasma accelerators. *Rev. Sci. Instrum*. **81** (3), 033108.

POMMAREL, L., VAUZOUR, B., MÉGNIN-CHANET, F., BAYART, E., DELMAS, O., GOUDJIL, F., NAURAYE, C., LETELLIER, V., POUZOULET, F., SCHILLACI, F., ROMANO, F., SCUDERI, V., CIRRONE, G.A.P., DEUTSCH, E., FLACCO, A. & MALKA, V. 2017 Spectral and spatial shaping of a laser-produced ion beam for radiation-biology experiments. *Phys. Rev. Accel. Beams* **20**, 032801.

PUYUELO-VALDES, P., HENARES, J.L., HANNACHI, F., CECCOTTI, T., DOMANGE, J., EHRET, M., D'HUMIERES, E., LANCIA, L., MARQUÈS, J.-R., RIBEYRE, X., SANTOS, J.J., TIKHONCHUK, V. & TARISIEN, M. 2019*a* Proton acceleration by collisionless shocks using a supersonic H2 gas-jet target and high-power infrared laser pulses. *Phys. Plasmas* **26** (12), 123109.

PUYUELO-VALDES, P., HENARES, J.L., HANNACHI, F., CECCOTTI, T., DOMANGE, J., EHRET, M., D'HUMIERES, E., LANCIA, L., MARQUÈS, J.-R., SANTOS, V. & TARISIEN, M. 2019b Laser driven ion acceleration in high-density gas jets. In *Proceedings of SPIE 11037, Laser Acceleration of Electrons, Protons, and Ions V*, p. 110370B. SPIE.

https://doi.org/10.1017/S0022377823001332 Published online by Cambridge University Press

Puyuelo-Valdes, P., de Luis, D., Hernandez, J., Apiñaniz, J.I., Curcio, A., Henares, J.L., Huault, M., Pérez-Hernández, J.A., Roso, L., Gatti, G. & Volpe, L. 2022 Implementation of a thin, flat water target capable of high-repetition-rate mev-range proton acceleration in a high-power laser at the clpu. *Plasma Phys. Control. Fusion* **64** (5), 054003.

Radier, C., Chalus, O., Charbonneau, M., Thambirajah, S., Deschamps, G., David, S., Barbe, J., Etter, E., Matras, G., Ricaud, S., *et al.* 2022 10 pw peak power femtosecond laser pulses at eli-np. *High Power Laser Sci. Engng* **10**, e21.

Rehwald, M., *et al.* 2023 Ultra-short pulse laser acceleration of protons to 80 mev from cryogenic hydrogen jets tailored to near-critical density. *Nat. Commun.* **14**, 4009.

Roso, L. 2018 High repetition rate petawatt lasers. *Eur. Phys. J. Web Conf.* **167**, 01001.

Rovige, L., Huijts, J., Vernier, A., Andriyash, I., Sylla, F., Tomkus, V., Girdauskas, V., Raciukaitis, G., Dudutis, J., Stankevic, V., Gecys, P. & Faure, J. 2021 Symmetric and asymmetric shocked gas jets for laser-plasma experiments. *Rev. Sci. Instrum.* **92** (8), 083302.

Salgado-López, C., Apiñaniz, J.I., Henares, J.L., Pérez-Hernández, J.A., de Luis, D., Volpe, L. & Gatti, G. 2022 Angular-resolved thomson parabola spectrometer for laser-driven ion accelerators. *Sensors* **22** (9).

Sarkisov, G.S., Bychenkov, V.Y., Novikov, V.N., Tikhonchuk, V.T., Maksimchuk, A., Chen, S.Y., Wagner, R., Mourou, G. & Umstadter, D. 1999 Self-focusing, channel formation, and high-energy ion generation in interaction of an intense short laser pulse with a he jet. *Phys. Rev.* E - *Stat. Phys. Plasmas Fluids Relat. Interdiscip. Topics* **59** (6), 7042–7054.

Silva, L.O., Marti, M., Davies, J.R., Fonseca, R.A., Ren, C., Tsung, F.S. & Mori, W.B. 2004 Proton shock acceleration in laser-plasma interactions. *Phys. Rev. Lett.* **92**, 015002.

Singh, P.K., Pathak, V.B., Shin, J.H., Choi, I.W., Nakajima, K., Lee, S.K., Sung, J.H., Lee, H.W., Rhee, Y.J., Aniculaesei, C., Kim, C.M., Pae, K.H., Cho, M.H., Hojbota, C., Lee, S.G., Mollica, F., Malka, V., Ryu, C.M., Kim, H.T. & Nam, C.H. 2020 Electrostatic shock acceleration of ions in near-critical-density plasma driven by a femtosecond petawatt laser. *Sci. Rep.* **10** (1), 1383–1386.

Spencer, I., Ledingham, K.W.D., Singhal, R.P., McCanny, T., McKenna, P., Clark, E.L., Krushelnick, K., Zepf, M., Beg, F.N., Tatarakis, M., Dangor, A.E., Norreys, P.A., Clarke, R.J., Allott, R.M. & Ross, I.N. 2001 Laser generation of proton beams for the production of short-lived positron emitting radioisotopes. *Nucl. Instrum. Meth. Phys. Res. Sec.* B*: Beam Interact. Mater. Atoms* **183** (3), 449–458.

Sylla, F., Flacco, A., Kahaly, S., Veltcheva, M., Lifschitz, A., Malka, V., d'Humières, E., Andriyash, I. & Tikhonchuk, V. 2013 Short intense laser pulse collapse in near-critical plasma. *Phys. Rev. Lett.* **110**, 085001.

Sylla, F., Veltcheva, M., Kahaly, S., Flacco, A. & Malka, V. 2012 Development and characterization of very dense submillimetric gas jets for laser-plasma interaction. *Rev. Sci. Instrum.* **83** (3), 033507.

Tresca, O., Dover, N.P., Cook, N., Maharjan, C., Polyanskiy, M.N., Najmudin, Z., Shkolnikov, P. & Pogorelsky, I. 2015 Spectral modification of shock accelerated ions using a hydrodynamically shaped gas target. *Phys. Rev. Lett.* **115**, 094802.

Wei, M.S., Mangles, S.P.D., Najmudin, Z., Walton, B., Gopal, A., Tatarakis, M., Dangor, A.E., Clark, E.L., Evans, R.G., Fritzler, S., Clarke, R.J., Hernandez-Gomez, C., Neely, D., Mori, W., Tzoufras, M. & Krushelnick, K. 2004 Ion acceleration by collisionless shocks in high-intensity-laser–underdense-plasma interaction. *Phys. Rev. Lett.* **93**, 155003.

Wilks, S.C., Kruer, W.L., Tabak, M. & Langdon, A.B. 1992 Absorption of ultra-intense laser pulses. *Phys. Rev. Lett.* **69**, 1383–1386.

Wilks, S.C., Langdon, A.B., Cowan, T.E., Roth, M., Singh, M., Hatchett, S., Key, M.H., Pennington, D., MacKinnon, A. & Snavely, R.A. 2001 Energetic proton generation in ultra-intense laser–solid interactions. *Phys. Plasmas* **8** (2), 542–549.

Yoon, J.W., Kim, Y.G., Choi, I.W., Sung, J.H., Lee, H.W., Lee, S.K. & Nam, C.H. 2021 Realization of laser intensity over 10^{23} w/cm2. *Optica* **8** (5), 630–635.

https://doi.org/10.1017/S0022377823001332 Published online by Cambridge University Press